Self-assembly of structured colloidal gels for high resolution 3D micropatterning of proteins at scale

Roxanna Ramnarine S, Janos M Kanczler, Nicholas D Evans, Richard OC Oreffo and Jonathan I Dawson

[1]Faculty of Medicine, Department of Human Development and Health, University of Southampton. SO16 6YD, UK.
***e-mail: jid@soton.ac.uk**

Abstract

Self-assembly, the spontaneous ordering of components into patterns, is widespread in nature and fundamental to generating function across length scales. Morphogen gradients in biological development are paradigmatic as both products and effectors of self-assembly and various attempts have been made to reproduce such gradients in biomaterial design. To date, approaches have typically utilised top-down fabrication techniques which, while allowing high resolution control, are limited by scale and require chemical cross-linking steps to stabilise morphogen patterns in time. Here, we develop a bottom-up approach to protein patterning based on a novel binary reaction-diffusion process where protein's function as diffusive reactants to assembly a nanoclay-protein composite hydrogel. Using this approach, we were able to generate scalable and highly stable 3D patterns of target proteins down to sub-cellular resolution through only physical interactions between clay nanoparticles and the proteins and ions present in blood. Patterned nanoclay gels were able to guide cell behaviour to precisely template bone tissue formation *in vivo*. Our results demonstrate the feasibility of stabilising 3D gradients of biological signals through self-assembly processes and open up new possibilities for morphogen-based therapeutic strategies and models of biological development and repair.

Keywords: self-organisation, diffusion-reaction, nanoparticles, protein delivery, 3D micropatterning

Introduction:

Developmental and regenerative studies agree that spatio-temporal patterns of biomacromolecules present in the extracellular matrix (ECM) direct cell function toward the assembly of hierarchical structures[1,2,3]. Recapitulation of spatially controlled presentation of biochemical cues is of value for fundamental studies of biological development and is likely to be key in the regeneration of functional tissues in medicine. Hydrogels are a promising candidate material in this context since their hydrated polymeric networks can emulate the viscoelastic properties of the ECM and potentially allow for loading of large quantities of protein[4]. Achieving patterning in hydrogels is difficult however, as it requires overcoming the fluctuations inherent to their high-water content.

To date, the traditional drug delivery paradigm of slow-release has dominated attempts to control presentation of biomolecules by hydrogel scaffolds. However, slow-release strategies are poorly suited to achieving the precisely defined protein gradients at play in natural morphogenesis. More

This article has been accepted for publication and undergone full peer review but has not been through the copyediting, typesetting, pagination and proofreading process, which may lead to differences between this version and the Version of Record. Please cite this article as doi: 10.1002/adma.202304461.

recent approaches to stabilising high-resolution 3D patterning of proteins in hydrogels have relied on top-down assembly methods such as photopatterning[5], electrophoresis[6], 3D printing[7] and microfluidics[8]. While these various approaches have demonstrated their utility for control of cell functions such as cell adhesion, migration and differentiation they each face challenges of scale-up, stability, protein activity and biocompatibility. Alternatively, various diffusion-based patterning systems have been applied to generate 3D gradients but these lack the resolution and complexity of direct patterning methods and face the same challenges of stability over time[9–11]. Furthermore, the *in vivo* utility of each of these methods remains largely untested.

In biological development, protein gradients are themselves a product of self-assembly processes. Since Alan Turing published his seminal work on the subject in 1952, the explanatory power of reaction-diffusion (RD) models for morphogen patterning in biology has been the subject of numerous analytic, computational and experimental studies[12,13,14]. However, as yet, the potential to exploit RD for engineering morphogen gradients remains unexplored[15]. In the present study, we demonstrate the utility of a simple binary RD system involving physical interactions between an arrested nanoclay colloidal gel and diffusing proteins to assemble stable patterning of bioactive proteins within a structured protein-clay nanocomposite hydrogel.

The nanoclay used in this study is the synthetic hectorite LAPONITE® a lithium magnesium sodium silicate ($Na_{0.7}^{+}[(Si_8Mg_{5.5}Li_{0.3})O_{20}(OH)_4]^{-0.7}$) consisting of rigid disk-shaped particles of approximately 25 nm diameter and 1 nm thickness (Fig. 1a). Owing to its chemical structure it possesses a negative face charge and a weak positive rim charge at neutral pH[16]. Laponite particles form delaminated dispersions in water via osmotic swelling and generate unique rheological properties due to the charge anisotropy of the particles which are subject to a range of mutual repulsive (face-to-face, edge–edge) and attractive (face to edge) electrostatic interactions[17]. These interactions and the resultant structure and properties of the colloid are highly sensitive to changes in ionic concentration, pH, and the presence of organic compounds[18]. We have previously described formation of stable, transparent protein-clay gels following the introduction of a viscous arrested nanoclay colloid into blood serum. We have also demonstrated the utility of such gels to bind and deliver growth factors to sustain localised concentrations *in vivo* to initiate regenerative responses[19,20]. Here we characterise Laponite gelation in proteins as a RD process and demonstrate how control over this process allows for stable protein patterning.

Results:

Assembly of 3D protein patterning in nanoclay gels was observed upon casting a viscous clay-gel suspension into a concentrated protein solution (such as blood serum or bovine serum albumin (BSA)) before transfer to a lower concentration solution of fluorescently labelled protein (e.g., FITC-BSA, in the order of 10-100 μg/ml) (Fig. 1b). This resulted in a transparent gel, of dimensions and shape controlled by the initial casting, containing a sharply defined band of fluorescent protein arrested between the gel periphery and its core (Fig. 1b - d and supplementary Fig. 1). Once assembled, patterning was found to be unusually stable, with gels immersed in a saline solution displaying negligible change in distribution or fluorescent intensity of the labelled protein even after several years of storage (Supplementary Fig. 2).

Subsequent confocal studies where FITC-BSA was loaded without, concurrent with, or (as above) after assembly in high concentration BSA, revealed a clear correspondence between the diffusion front of the concentrated protein solution and the localisation of the labelled protein (Fig. 2a) indicating a process of progressive saturation and specific binding at the diffusion front. The sharply

defined diffusion front is a notable feature of the system and suggestive of a reaction diffusion process[21]. We posited that during the first step (assembly), the high concentration protein proceeds via diffusion into the arrested clay gel, saturating the clay nanoparticles and restructuring the gel into a protein-clay composite network (Fig. 2b, see also Fig. 2a, middle column). In the second step (loading), the new reacted protein-clay phase, now saturated by protein, facilitates specific protein binding at the first available unreacted region of clay to create (along with some non-specific binding at the gel surface) a sharply defined protein band at the diffusion front (Fig. 2b, see also Fig. 2a right column).

Hydrogels assembled via a RD process, also known as physical hydrogels, develop characteristic structural features which include, in addition to a distinctive diffusion front, anisotropic arrangements[22], parallel or perpendicular reorientation of the particles with respect to the diffusion front or flux[23], re-arrangement of the porous network[21] and internal redistribution of the particle density[24]. These features can be studied with a range of imaging techniques, such as brightfield (BF), polarised light microscopy (PLM), and transmission and scanning electron microscopy (TEM and SEM), and all were observable in the protein-clay composite. Under BF, while both reacted and unreacted regions remained transparent, a clearly observable interface at the diffusion front was indicative of a phase transition (Fig. 2c). Under PLM, when diffusion was limited to a single plane, a strong and radial birefringence was observed in the reacted-clay region (Fig. 2d). A slight polarisation was also apparent in the unreacted clay region following autoclave sterilisation, but this order was not, we confirmed, required for birefringence arising from RD (Supplementary Fig. 3). Anisotropic ordering was further examined by TEM, under which Laponite nanoparticles present as spindles of about ~25 nm length[25] due to their low mass thickness contrast when viewed parallel to the planar surface (Fig. 2e). Analysis of the particle orientation distribution on the visible axial plane revealed, in the reacted region, preferential alignment perpendicular to the direction of diffusion. We also observed, via particle counts per TEM micrograph frame, a slight increase in the average particle density in the reacted region suggesting some translation of particles counter to the direction of the progressing front in service of the protein-clay complex (Supplementary Fig. 4). Finally, SEM imaging indicated changes in the microstructure where the reacted region presents as a porous network of fibres and the unreacted remains as a dense granular structure comparable to the pristine clay-gel (Fig. 2f and Supplementary Fig. 5).

These structural features and the process by which they form, indicate a binary RD system. Broadly, a binary RD system is one in which diffusive molecules and a static phase that are initially separated in space, react and develop a diffusion front, the propagation of which leaves behind a reaction product[26]. Several synthetic and naturally occurring macromolecules can self-assemble via binary RD. These types of assemblies typically require a semi-rigid or rigid charged macromolecule[27] to form a static phase (examples include: poly-2,2´-disulfonyl-4,4´-benzidine terephthalamide (PBDT)[21], alginate[22], κ-Carrageenan[28], carboxymethylcellulose[29], DNA, fibril proteins[30], chitosan[31] and curdlan[32]) which then self-assemble in response to the diffusion of multivalent ions[7]. To our knowledge this is the first demonstration of an RD assembly system involving an arrested inorganic phase and - perhaps more significantly - where large macromolecules rather than ions constitute the diffusive reactant. It is this feature in particular, facilitated by the very high sorptive capacity of clay[19], that provides the opportunity to achieve 3D patterning of the loaded protein.

Since the nanoclay-protein gel assembly is the result of a RD process, we expected that characterization of the key parameters known to affect diffusion (concentration, temperature, and time) and clay-protein interactions (such as ionic strength and pH), would enable control of the diffusion front and resultant protein patterning. Correspondingly, the RD rate – as indicated by a

progressing diffusion front over time – shows direct dependency on the protein concentration of the assembly solution which continues over time until either complete saturation or upon removal from the assembly solution at which point the RD front is arrested (Fig. 3a and 3c). Variation of the incubation time and protein concentration confirm a linear relationship between the protein diffusion depth and the square root of time, independent of protein concentration (Supplementary Fig. 6). As expected, assembly at 37^{o}C accelerates the displacement of the diffusion front compared to 4^{o}C (Supplementary Fig. 7).

We found the ionic strength of the assembly solution to be particularly important for the stability of the reacted gel. Notably, BSA alone in salt-free dH_20 is, in fact, sufficient to initiate a RD front and sustain gelation, an observation which provides further confirmation that a nanoclay-protein complex forms as a reaction product. However, an RD front is observed only at a relatively high protein concentration (~20 mg/ml). Below this threshold the rate of swelling of the arrested nanoclay, exceeds the rate of RD and the gel dissipates prior to formation of the clay protein assembly (Fig 3b). The inclusion of ions, either prior to or concurrent with addition of protein, stabilises the gel network so that a RD front can be generated at lower protein concentrations (<5 mg/ml) (Fig. 3a and Supplementary Fig. 8). Furthermore, whereas in the presence of salt the linear dimensions of the gel remain very stable over the entire course of the RD process, in BSA alone the progress of the RD front correlates with a progressive shrinkage of the gel dimensions (Supplementary Fig. 9). This indicates a further stabilising influence of ions against protein-driven contraction of the gel network. Finally, increasing ionic concentration exerted a slight influence on the RD rate where an increase in salt concentration up to ~50 mM correlated with faster progression of the RD front (Supplementary Fig. 10).

It is notable that both the ionic and protein concentrations applied in these experiments go well above the threshold at which Laponite suspensions characteristically undergo flocculation induced phase separation in simple mixed systems[33]. Such flocculation is caused by cation-induced compression of the negative electric double layer on the particle surface and a resultant accumulation of face to edge attractive interactions between particles. We have previously proposed a diffusion gelation mechanism in which a progressively increasing solute concentration across an arrested nanoclay phase causes local reorientation and electrostatic bonding of particles into a stable gel network, resistant to further translation of particles into large-scale flocculates[34]. The current results are broadly consistent with this conceptualisation but indicate discrete contributions of ions and proteins. While ion diffusion plays a role in stabilising the network, the formation of the sharply defined diffusion front indicates that threshold concentrations of diffusing proteins effect a further phase transition in the gel structure. Further experimental and theoretical studies are warranted to characterise these interactions and the anisotropic structures that result.

The influence of pH on gel assembly appears more subtle and is likely to be protein specific. In the case of BSA, like ionic concentration, increasing pH between pH4 and pH10 correlated with a slight but significant increase in the rate of progression of the RD front (Supplementary Fig. 10), but unlike ionic concentration did not effect a significant change in the gel dimensions over an equivalent time frame ($p = 0.516$). Both ionic strength and pH effects on protein-clay interactions are complex and change both system components in a variety of non-linear ways. The increase in rate of front progression with pH and salt concentration would be consistent with a reduction in the saturation capacity of clay surfaces due to steric effects arising from protein conformational changes or else altered electrostatic profiles[35,36].

Thus, pre-treatment of a Laponite colloid with high concentration BSA protein in a salt buffer causes a change in state of the Laponite (to the reacted state) which then allows patterning of a

subsequently added protein at the reaction front. To determine if the induction of the reacted state was specific to BSA or could be extrapolated across a wider range of proteins, we next performed assembly with various globular proteins across a spectrum of isoelectric points (4 - 10) and molecular weights (14 - 150 kDa) before loading with FITC-BSA. In every case a distinct diffusion front was generated, although the RD rate varied significantly between proteins, along also with the opacity of the reacted gel (Supplementary Fig. 11). Interestingly, the rate correlated poorly with either protein size or net charge and further work is therefore required to understand the specific parameters influencing each protein's RD rate in this system, as well as the effect of different proteins on the reacted gel structure.

The ability to load alternative proteins at the reaction front once assembled, appears to be dependent principally on the charge of the loaded protein in relation to that of the assembling protein (Fig. 4a). So, for example, in gels assembled in lysozyme, loaded lysozyme (isoelectric point, 11.35) localised at the diffusion front whereas in gels assembled in BSA (isoelectric point, 4.7), lysozyme binding was limited to the gel surface – a result also observed when BSA was loaded into lysozyme assembled gels (Fig. 4a). These results imply a selective diffusion process governed by electrostatic interactions between the protein-clay complex and the loaded proteins in which attractive interactions hinder diffusion and repulsive interactions facilitate it. Correspondingly, we found that lysozyme loading at the reaction front could be achieved even in a BSA-assembled gel by lowering the pH of the assembly buffer to the point where both BSA and lysozyme were positively charged (Fig. 4b). A related effect of pH on loading was the observation that the "non-specific" binding of FITC BSA at the gel surface (as opposed to at the diffusion front; cf. Fig. 1c) could be eliminated by lowering the pH of the assembly solution (Supplementary Fig. 10). This non-specific surface binding can be accounted for by the altered charge-related surface properties of BSA when labelled with FITC (such as a lower isoelectric point (IEP) and increased hydrophobicity relative to native BSA). These changes are well characterised in the literature [37] and are sufficient to explain the secondary binding of a fraction of the loaded labelled protein within regions already reacted with unlabelled BSA. Attenuating these effects of FITC labelling by lowering the pH towards the protein IEP thus also attenuates secondary binding.

As noted, the use of proteins as diffusive reactants presents an exciting opportunity for protein patterning through scalable, bottom-up assembly methods. By effecting a controllable phase transition in the colloidal gel structure, proteins can be stably 'written-in' by the progressing RD front allowing a unique degree of control and stability not achievable with other diffusion-based hydrogel functionalisation strategies[9,10]. Thus, by timed introduction into the assembly solution, loaded proteins can be patterned into the assembled gel at both very high concentrations (in the order of tens of milligrams per ml (Supplementary Fig. 13)) and at very high resolution. It was relatively simple, for example, by lowering the assembly protein concentration to slow the RD rate to achieve protein band thickness and spacing at sub-cellular resolutions approaching that of two-photon patterning, the current state of the art[38] (Fig. 4e and 4f).

Unusually for a physical hydrogel, we found that once incorporated at the RD front, loaded proteins can remain localised for extended periods in ionic solution without being displaced even under agitation (Supplementary Fig. 2 and 12). This high degree of stability, while not fully understood, is consistent with the high sorption capacity of clays for proteins as well as their well-established ability to stabilise biomolecules through surface binding – a phenomena of known significance in soil ecosystems[39].

By controlling the order of introduction, timing and concentration of loaded protein with respect to the assembly process, it was possible to generate a range of conformations of protein patterning. So,

for example, gels of multiple, punctuated bands of loaded protein could be achieved by repeatedly alternating high protein concentration assembly steps with lower concentration loading steps. With careful timing and buffer selection, alternating bands of different proteins could also be achieved using this approach (Fig. 4c). Similarly, by gradually changing the concentration of loaded protein within the assembly solution over the course of the RD process, continuous gradients of varying magnitude (depending on rate of change) and dual gradients of simultaneously increasing and decreasing protein concentrations, could be patterned with high reproducibility within the gel structure (Fig. 4d).

Finally, we sought to test the ability of a protein patterned through the RD system to induce a biological response. Our previous work[20] has demonstrated the utility of nanoclay gels for sustaining and localising the activity of the bone inducing morphogen, bone morphogenic protein 2 (BMP-2) *in vivo* and so here the ability of RD patterned BMP-2 to template bone formation was tested. BMP-2 was labelled with Dylight 633 to allow visualisation of patterning within the gel and activity was confirmed using the C2C12 dose response assay (Supplementary Fig. 14). A serendipitous finding of this study was that labelling with the negatively charged Dylight molecule was itself sufficient to allow patterning, even at neutral pH, of the otherwise positively charged BMP-2 protein (pI = 8.5) within a BSA assembled gel (Supplementary Fig. 15). BSA RD gels were patterned with a sharply defined band of BMP-2 spatially distinct from the gel surface (Fig. 5b). We would stress that the purpose of this design was specifically to test the hypothesis that resultant bone induction conforms to the geometry of the patterned BMP-2 and was not intended as a biological optimum for BMP-2 delivery. Patterned BMP-2 gels were assessed for bone induction in a murine subcutaneous ectopic bone induction assay against gels in which an equivalent concentration of BMP-2 + BSA was mixed homogenously throughout the gel volume. µCT and histological analysis revealed bone formation in 4/5 patterned samples but only 2/5 mixed gels within the 8-week time frame (Supplementary Fig. 16). As well as differences in BMP2 distributions which yields an approximately 6x higher local concentration within patterned regions of the RD gels, we also noted that the mixed preparations displayed a lower elastic modulus which may also be a relevant difference affecting bone forming efficiency (Supplementary Fig. 17). No bone was present in the absence of BMP-2.

Histological analysis confirmed new bone spicule formation proximal to the implanted gel volume (Fig. 5d, and Supplementary Fig.17) Critically, region of interest analysis of bone formation in 8-week explants confirmed >90% of bone in the patterned gels localised to within 0.4 mm of the expected BMP-2 region (compared with <5% in the mixed gels) (Fig. 5e). Furthermore, where sufficient bone tissue permitted measurement of curvature (n=3), the geometry of the bone tissue conformed tightly to the that of the labelled protein imaged prior to implantation (Fig. 5g). These results thus provide strong evidence for the ability of RD gels to pattern active BMP-2 to guide bone formation *in vivo*.

Conclusions:

In summary, we have reported a new binary reaction-diffusion system where, uniquely, macromolecules rather than multivalent ions function as the diffusive reactant to restructure an arrested inorganic colloid into a stable gel. Employing this phenomenon we show how, through timed introduction over the course of the reaction-diffusion process, functional proteins can be stably patterned into the resultant gel structure and demonstrate the utility of this approach for patterning the morphogen BMP-2 to template bone induction *in vivo.* The approach has significant advantages. As a bottom-up self-assembly method, patterning is highly scalable and can be achieved under physiological and biocompatible conditions, free of chemical cross-linkers and employing only (if

necessary) clay interactions with proteins and ions present in blood. Active proteins can be patterned at resolutions comparable to the limits of current fabrication techniques, at concentrations in the order of tens of milligrams per ml and with patterns remaining stable in solution over several years. These advantages, combined with the established ability of nanoclays to enhance growth factor bioactivity *in vivo*, suggest exciting potential for high-resolution control of biological function at clinically relevant scale.

Materials and methods:

All experiment details are provided in the supporting information.

References

1. Zagorski, M. *et al.* Decoding of position in the developing neural tube from antiparallel morphogen gradients. *Science (1979)* **356**, 1379–1383 (2017).
2. Dathe, K. *et al.* Duplications Involving a Conserved Regulatory Element Downstream of BMP2 Are Associated with Brachydactyly Type A2. *Am J Hum Genet* **84**, 483–492 (2009).
3. Wilson, C. G., Martín-Saavedra, F. M., Vilaboa, N. & Franceschi, R. T. Advanced BMP gene therapies for temporal and spatial control of bone regeneration. *J Dent Res* **92**, 409–417 (2013).
4. Bae, K. H. & Kurisawa, M. Emerging hydrogel designs for controlled protein delivery. *Biomater Sci* **4**, 1184–1192 (2016).
5. Mosiewicz, K. A. *et al.* In situ cell manipulation through enzymatic hydrogel photopatterning. *Nat Mater* **12**, 1072–1078 (2013).
6. Aguilar, J. P. *et al.* 3D Electrophoresis-Assisted Lithography (3DEAL): 3D Molecular Printing to Create Functional Patterns and Anisotropic Hydrogels. *Adv Funct Mater* **28**, 1–10 (2018).
7. Liu, W. *et al.* Rapid Continuous Multimaterial Extrusion Bioprinting. *Advanced Materials* **29**, 1–8 (2017).
8. Lee, U. N. *et al.* Layer-by-layer fabrication of 3D hydrogel structures using open microfluidics. *Lab Chip* **20**, 525–536 (2020).
9. Kamperman, T. *et al.* Spatiotemporal material functionalization via competitive supramolecular complexation of avidin and biotin analogs. *Nat Commun* **10**, 4347 (2019).
10. Yi, Z., Zhang, Y., Kootala, S., Hilborn, J. & Ossipov, D. A. Hydrogel Patterning by Diffusion through the Matrix and Subsequent Light-Triggered Chemical Immobilization. *ACS Appl Mater Interfaces* **7**, 1194–1206 (2015).

11. Li, C. *et al.* Buoyancy-Driven Gradients for Biomaterial Fabrication and Tissue Engineering. *Advanced Materials* **31**, 1900291 (2019).

12. Turing, A. M. The chemical basis of morphogenesis. *Philos Trans R Soc Lond B Biol Sci* **237**, 37–72 (1952).

13. Epstein, I. R. & Xu, B. Reaction–diffusion processes at the nano- and microscales. *Nat Nanotechnol* **11**, 312–319 (2016).

14. Kondo, S. & Miura, T. Reaction-Diffusion Model as a Framework for Understanding Biological Pattern Formation. *Science (1979)* **329**, 1616–1620 (2010).

15. Grzybowski, B. A., Bishop, K. J. M., Campbell, C. J., Fialkowski, M. & Smoukov, S. K. Micro- and nanotechnology via reaction–diffusion. *Soft Matter* **1**, 114 (2005).

16. Mousa, M., Evans, N. D., Oreffo, R. O. C. & Dawson, J. I. Clay nanoparticles for regenerative medicine and biomaterial design: A review of clay bioactivity. *Biomaterials* vol. 159 204–214 Preprint at https://doi.org/10.1016/j.biomaterials.2017.12.024 (2018).

17. Ruzicka, B. *et al.* Observation of empty liquids and equilibrium gels in a colloidal clay. *Nat Mater* **10**, 56–60 (2011).

18. Ruzicka, B. & Zaccarelli, E. A fresh look at the Laponite phase diagram. *Soft Matter* **7**, 1268 (2011).

19. Dawson, J. I., Kanczler, J. M., Yang, X. B., Attard, G. S. & Oreffo, R. O. C. Clay Gels For the Delivery of Regenerative Microenvironments. *Advanced Materials* **23**, 3304–3308 (2011).

20. Gibbs, D. M. R. *et al.* Bone induction at physiological doses of BMP through localization by clay nanoparticle gels. *Biomaterials* **99**, 16–23 (2016).

21. Wu, Z. L. *et al.* In situ observation of Ca2+ diffusion-induced superstructure formation of a rigid polyanion. *Macromolecules* **47**, 7208–7214 (2014).

22. Maki, Y. *et al.* Anisotropic structure of calcium-induced alginate gels by optical and small-angle X-ray scattering measurements. *Biomacromolecules* **12**, 2145–2152 (2011).

23. Ziemecka, I., Koper, G. J. M., Olive, A. G. L. & van Esch, J. H. Chemical-gradient directed self-assembly of hydrogel fibers. *Soft Matter* **9**, 1556–1561 (2013).

24. Voo, W.-P., Ooi, C.-W., Islam, A., Tey, B.-T. & Chan, E.-S. Calcium alginate hydrogel beads with high stiffness and extended dissolution behaviour. *Eur Polym J* **75**, 343–353 (2016).

25. Jatav, S. & Joshi, Y. M. Chemical stability of Laponite in aqueous media. *Appl Clay Sci* **97–98**, 72–77 (2014).

26. Bazant, M. Z. & Stone, H. A. Asymptotics of reaction-diffusion fronts with one static and one diffusing reactant. *Physica D* **147**, 95–121 (2000).

27. Wu, Z. L. & Gong, J. P. Hydrogels with self-assembling ordered structures and their functions. *NPG Asia Mater* **3**, 57–64 (2011).

28. Narita, T., Ohnishi, I., Tokita, M. & Oishi, Y. Macroscopic pattern formation of liquid crystal in κ-carrageenan gel. *Colloids Surf A Physicochem Eng Asp* **321**, 117–120 (2008).

29. Lin, S. C. *et al.* Phase relationship and dynamics of anisotropic gelation of carboxymethylcellulose aqueous solution. *Colloid Polym Sci* **288**, 695–701 (2010).

30. Furusawa, K. *et al.* Studies on the formation mechanism and the structure of the anisotropic collagen gel prepared by dialysis-induced anisotropic gelation. *Biomacromolecules* **13**, 29–39 (2012).

31. Sacco, P. *et al.* Insight into the ionotropic gelation of chitosan using tripolyphosphate and pyrophosphate as cross-linkers. *Int J Biol Macromol* **92**, 476–483 (2016).

32. Dobashi, T. *et al.* Liquid crystalline gel beads of Curdlan. *Langmuir* **21**, 2–4 (2005).

33. Mongondry, P., Tassin, J. F. & Nicolai, T. Revised state diagram of Laponite dispersions. *J Colloid Interface Sci* **283**, 397–405 (2005).

34. Shi, P. *et al.* Self-Assembling Nanoclay Diffusion Gels for Bioactive Osteogenic Microenvironments. *Adv Healthc Mater* **7**, (2018).

35. Quiquampoix, H. & Ratcliffe, R. G. *A 31p NMR Study of the Adsorption of Bovine Serum Albumin on Montmorillonite Using Phosphate and the Paramagnetic Cation Mn2+: Modification of Conformation with pH*. (1992).

36. Staunton, S. & Quiquampoix, H. Adsorption and Conformation of Bovine Serum Albumin on Montmorillonite: Modification of the Balance between Hydrophobic and Electrostatic Interactions by Protein Methylation and pH Variation. *J Colloid Interface Sci* **166**, 89–94 (1994).

37. Richert, M. E., García Rey, N. & Braunschweig, B. Charge-Controlled Surface Properties of Native and Fluorophore-Labeled Bovine Serum Albumin at the Air-Water Interface. *J Phys Chem B* **122**, 10377–10383 (2018).

38. Krüger, H., Asido, M., Wachtveitl, J., Tampé, R. & Wieneke, R. Sensitizer-enhanced two-photon patterning of biomolecules in photoinstructive hydrogels. *Commun Mater* **3**, (2022).

39. Schmidt, M. P. & Martínez, C. E. Kinetic and Conformational Insights of Protein Adsorption onto Montmorillonite Revealed Using in Situ ATR-FTIR/2D-COS. *Langmuir* **32**, 7719–7729 (2016).

Acknowledgements

We are grateful to the Engineering and Physical Sciences Research Council (EPSRC, EP/L010259/1 and EP/S017054/1) and the University of Southampton for funding the project. We thank members of the Biomedical Imaging Unit of the University of Southampton for with their help with sample processing, different imaging techniques used in this paper and 3D printing, particularly D. Johnstone, R. Doherty, K. Dexter, G. Patricia and A. Page. We also like to thank A. Janeczek and P. Duriez for advice with protein labelling and purification, J. Wells for histology sample processing and J. Van Duijneveldt for contribution with the diffusion profile analysis.

Author contribution

R.R.S. discovery, concept and design, carried out all patterning experiments in vitro and in vivo, collection and assembly of all data, data analysis and interpretation, manuscript writing, final approval of manuscript; J.K. in vivo studies and manuscript writing; R.O. design, data interpretation, manuscript writing; N.E. data interpretation and manuscript writing; J.D concept and design, data analysis and interpretation, manuscript writing and final approval of manuscript.

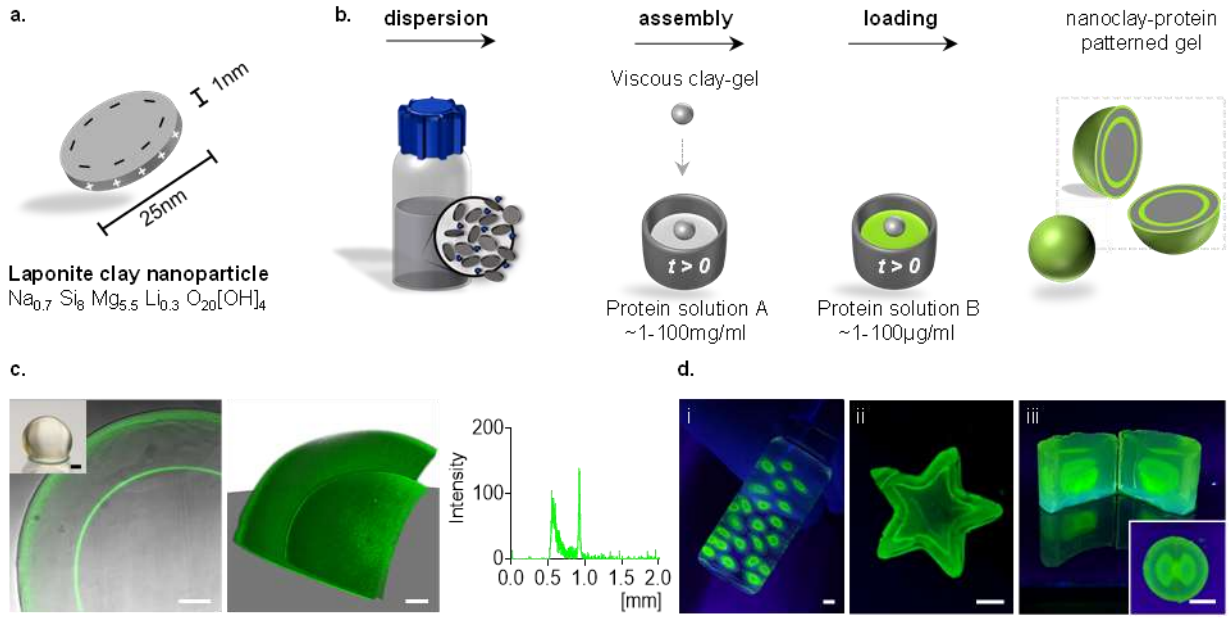

Figure 1. Assembly of 3D protein patterning within nanoclay colloidal gels. a, Laponite clay nanoparticles approximate 25nm disks of 1nm thickness and possess a permanent negative surface charge and a weak positive edge charge at neutral pH which form viscous colloidal dispersions in water above ~2 wt%. **b**, after drop casting a viscous dispersion of laponite into a high concentration protein solution (concentrations in the order of 1-100mg/ml) and then, after a given time, transferring the gel to a lower concentration solution (concentrations in the order of 1-100µg/ml) of labelled protein a sharply defined band of labelled protein within the gel was observed. **c**, for example, 3D reconstruction of confocal image and analysis of transparent gel droplets exposed to 10mg/ml BSA for 1 hour and then 100µg/ml FITC BSA for 1 hour reveals a sharp band of fluorescent protein patterned between the gel periphery and core (scale bar, 200µm), plot presents fluorescent intensity within a linear region of interest (running from top left to the bottom right of the image. **d**, the system supports the assembly and patterning of structures of a range of size and shapes as defined by the initial casting. For example, UV transilluminator images of (i) clay-gel droplets of 20µl incubated in 60% FCS PBS for 170min and then in 100µg/ml FITC BSA for 48h (scale bar, 200µm); (ii) 1ml clay-gel star-shape assembled in 50mg/ml BSA PBS for 4h and patterned with 500µg/ml FITC BSA for 24h; (iii) a segmented 1ml clay-gel cylinder assembled in 100% FCS for 72h and patterned with 250µg/ml FITC BSA for 96h (scale bars, 4mm). Similar results were obtained for n=3 independent samples.

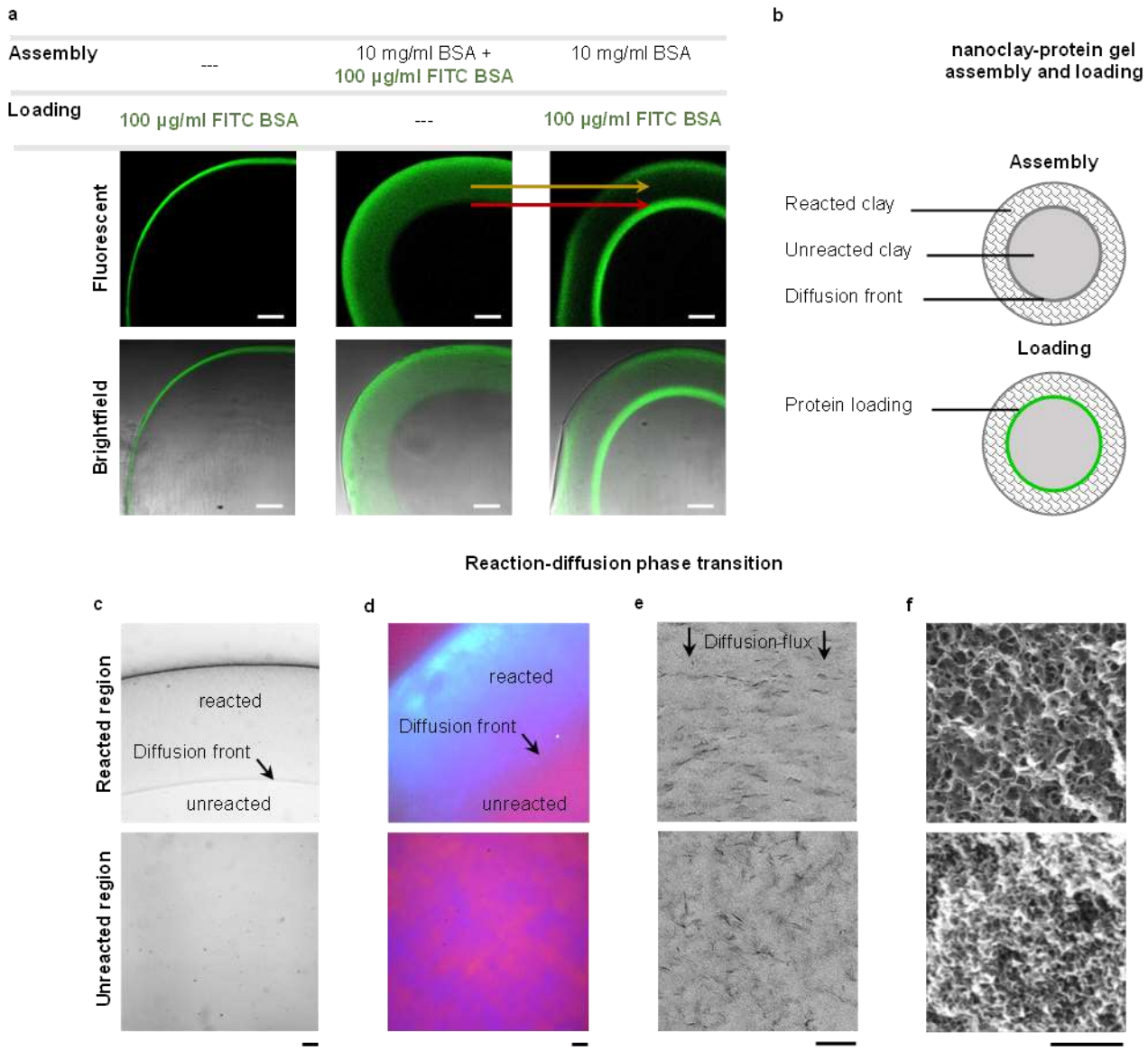

Figure 2. Reaction-diffusion phenomena in nanoclay-protein assembly and patterning. a, Confocal analysis of nanoclay colloidal gels loaded with FITC-BSA without, concurrent with, or after assembly in BSA (10 mg/ml). Inclusion of FITC BSA in the assembly solution reveals a protein gradient (yellow arrow) with a clear diffusion front (red arrow) that co-locates with the fluorescent band formed when FITC-BSA is loaded after assembly in BSA (n = 3, scale bars, 200µm). **b,** A Schematic illustration of the proposed nanoclay-protein assembly process in which high concentration protein progressively saturates the clay nanoparticles to facilitate specific binding of the loaded protein at the diffusion front. **d-f**, Microscopy analysis confirms a phase transition occurs behind the diffusion front. **c,** Bright field images of gels reveal the formation of an interface at the diffusion front indicative of a phase transition (n = 3, scale bars, 200µm). **d,** Polarised light microscopy reveals radial birefringence of the reacted clay region as well as threaded texture in the unreacted clay (n = 3, scale bars, 200µm). **e,** Transmission electron microscopy indicates a preferential orientation of the nanoparticles behind the diffusion front in contrast to a random orientation in the non-reacted region (n = 3, scale bars, 100nm). **f,** SEM shows a more open, porous structure in the reacted region compared to the unreacted core (n = 3, scale bars, 1µm).

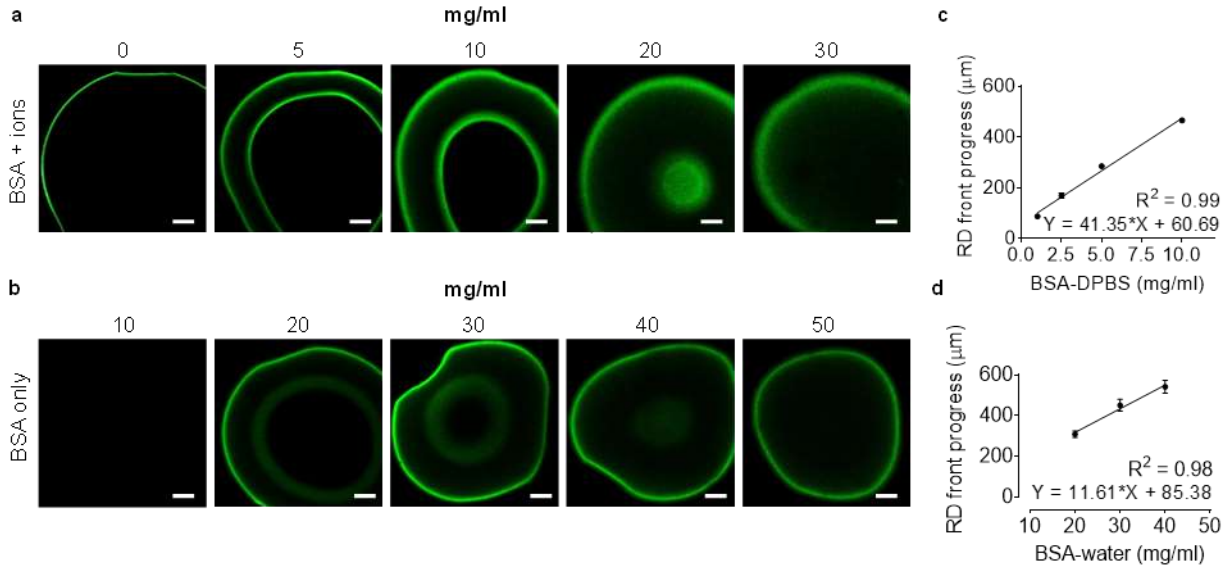

Figure 3. Nanoclay-protein gel reaction diffusion rate as a function of protein concentration and the presence of ions. a, Confocal micrographs reveal a first fluorescent band at the surface of all nanoclay-protein gel and a second fluorescent band that displaces towards the core with an increase in the protein concentration indicating a more rapid progression of the diffusion front. **b,** A diffusion front was also generated without salts, but only at protein concentrations of 20mg/ml or above as below this the arrested nanoclay dispersion swelled and dissipated prior to the formation of a clay-protein assembly. **c** and **d,** A linear regression indicate that the displacement of the internal fluorescent ring with and without ions is concentration dependent with an R^2 of 0.99 and 0.98, respectively. The results represent mean ± SD for n = 4 and the scale bars to 200µm.

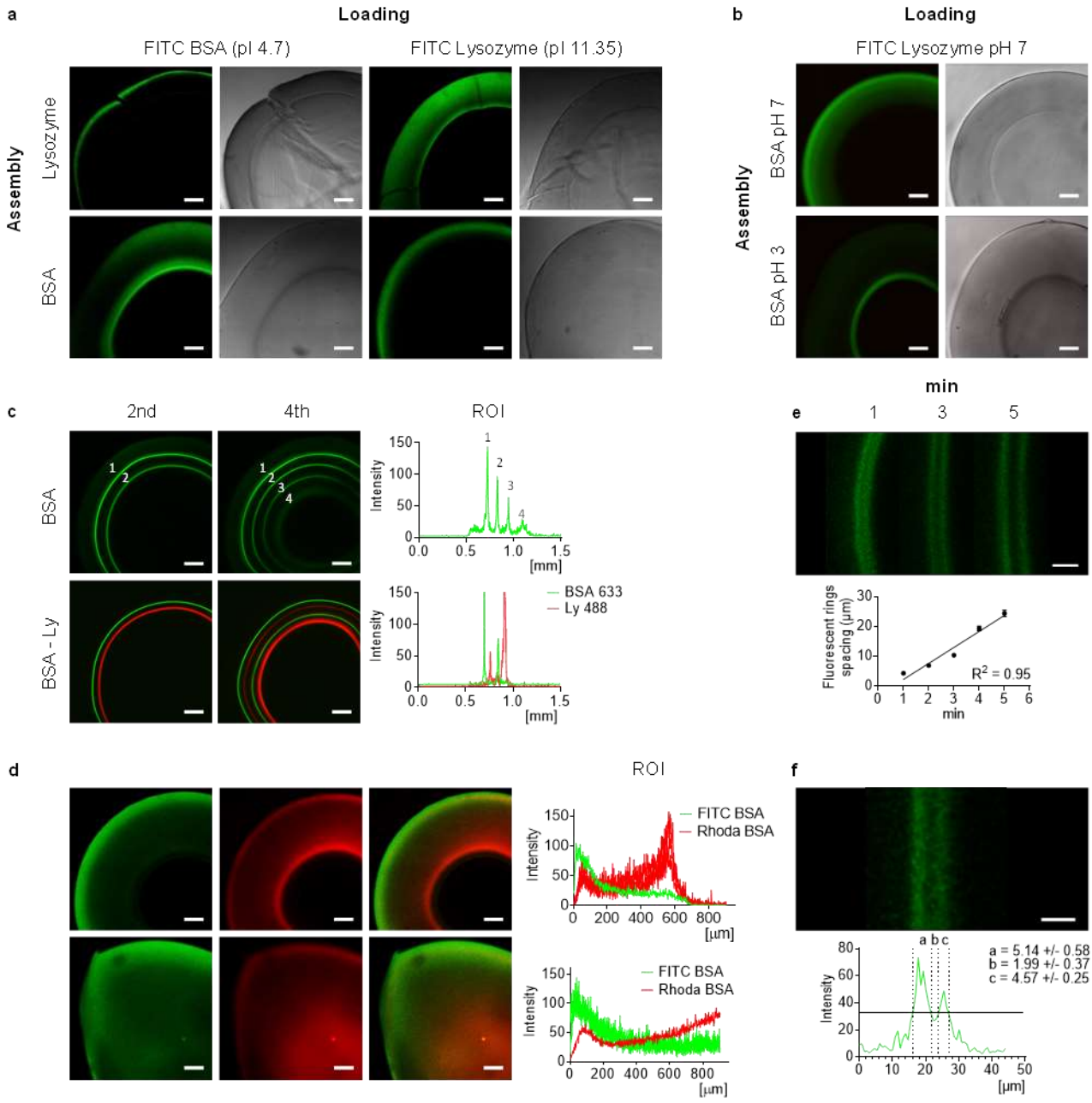

Figure 4. Versatility of nanoclay-protein gel patterning. a, The localisation of proteins at the diffusion front is driven by the charge of the loaded protein with respect to the charge of the protein used for nanoclay-protein gel assembly. BSA and lysozyme (10mg/ml) in PBS (pH 7.4) possess negative and positive net charges, respectively. When using the same type of protein for assembly and loading, the loaded protein (100µg/ml FITC BSA or FITC lysozyme) localised at the diffusion front, and when using oppositely charged proteins they localised at the gel surface. **b,** The protein charge of the assembly solution can be altered by adjusting the pH buffer to facilitate its diffusion to the diffusion front so in contrast to clay-gels assembled with BSA pH 7 which resulted in lysozyme binding only at the surface, gels assembled with BSA at pH 3 before exposure to FITC-lysozyme allowed lysozyme loading at the diffusion front. **c,** Proteins are stably bound within the reacted region allowing the creation of sequential protein bands by alternating the assembly and loading steps. Here scaffolds were loaded with repeated bands of FITC-BSA or with alternating bands of BSA (labelled with Alexa-633) and lysozyme (labelled with Alexa-488). **d,** Similarly, by changing the protein concentration of diffusive protein as a function of time both positive and negative gradients of varying magnitude could be simultaneously generated. **e - f,** Varying the assembly time allows a high degree of control over the localisation of loaded protein distribution, down to **f,** sub-cellular resolutions of band spacing (1.99 ± 0.37 µm) and thickness (4.6 ± 0.25 µm)**.** Images are representative of n = 3 and the scale bars a, b, c, d 200µm; e, 50µm and f, 10µm).

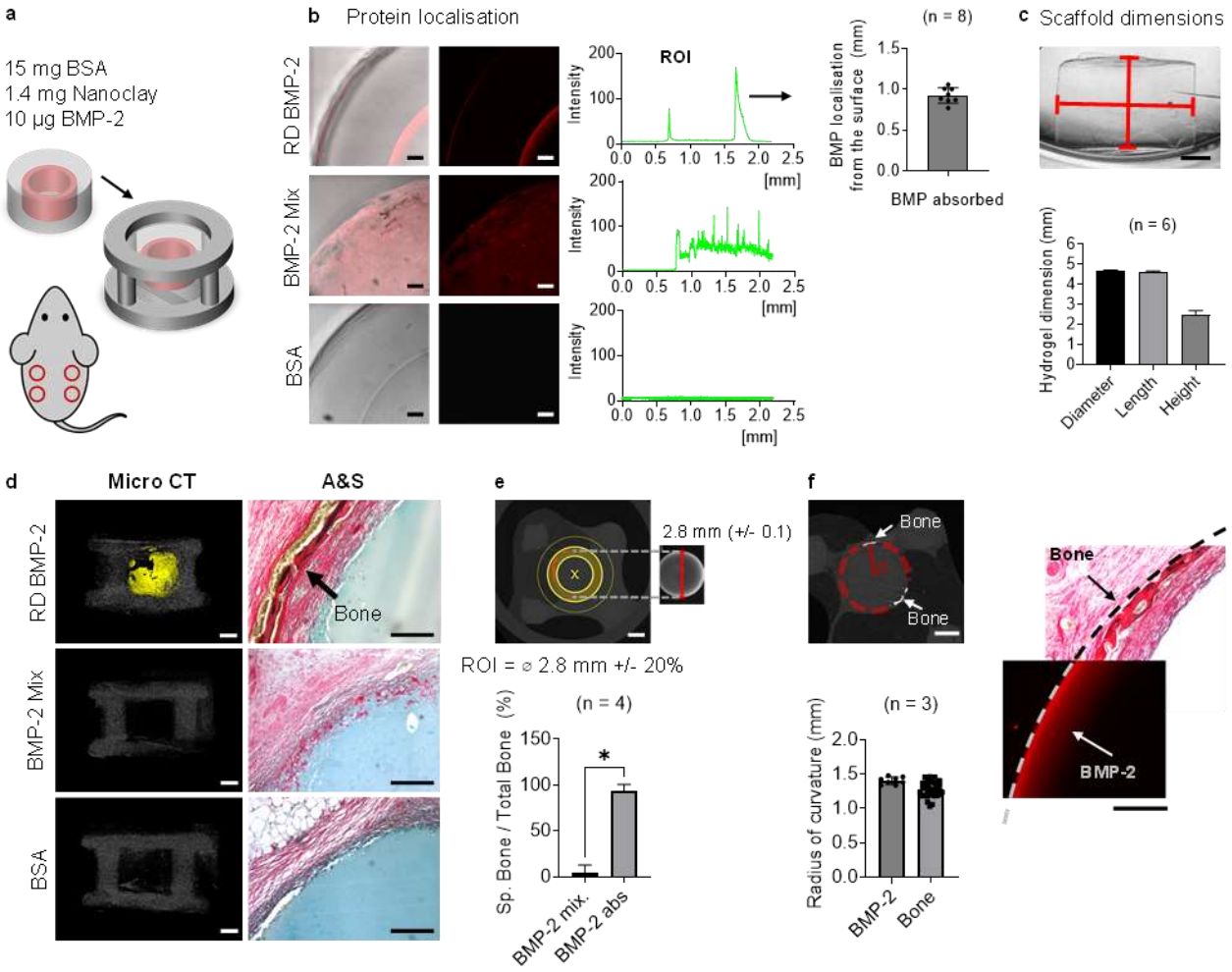

Figure 5. Reaction-diffusion patterning of BMP-2 templates ectopic bone induction. a, Nanoclay gels (50 µl) were assembled in BSA to pattern BMP-2 before murine subcutaneous implantation within a space retaining polylactic acid scaffold. RD patterned gels contained 9.95 ± 0.42 µg/ml BMP-2 (Dylight NHS 633, ELISA, n=2) and 15.89 ± 3.28 mg/ml BSA (protein assay, n = 3) and were compared with controls containing equivalent protein concentrations of either BMP-2 and BSA or BSA alone through mixing. **b,** Confocal micrographs and respective ROI show the spatial localization of labelled BMP-2 within the nanoclay-gels. RD patterned BMP2 was localised as a band 0.92 ± 0.09 mm from the gel surface (n=3, scale bar 200µm). **c,** The average structure diameter, length and height of the assembled was highly uniform (4.68 ± 0.04mm, 4.64 ± 0.03mm and 2.51 ± 0.18mm (n=6), scale bar 1mm). **d,** Robust formation of bone within the gel cylinder region in the patterned gels was apparent by week 4 post implantation (scale bar 1mm). Alcian blue/Sirius red (A/S) staining confirms cell invasion and a distinct band of ectopic bone formation within the patterned gel (scale bar 200µm). **e,** Micro CT analysis of specific bone within the expected ROI (⌀ 2.8 mm +/- 20%) reveals more bone formation over the projected area of the BMP-2 pattern compared to the positive control (n=3, scale bar 1mm). **f,** Measurement of the bone curvature corresponds closely with that of the BMP-2 pattern observed prior to implantation as confirmed through CT analysis (n=3, scale bar 1mm) and illustrated against Sirius red staining of new bone (scale bar 200µm).

We report a new reaction diffusion self-assembly system in which proteins function as diffusive reactants to assemble stable clay-protein composite hydrogels. We demonstrate the opportunity to exploit this system to assemble stable 3D patterning of bioactive proteins with high protein loading, resolution and scalability.